Faraday Discussions

Cite this: *Faraday Discuss.*, 2017, **199**, 9

PAPER

View Article Online
View Journal | View Issue

Chemical physics of electroactive materials – the oft-overlooked faces of electrochemistry

Zinaida A. Kostiuchenko,†[a] Piotr J. Glazer,†[b] Eduardo Mendes[b] and Serge G. Lemay*[a]

Received 27th March 2017, Accepted 13th June 2017
DOI: 10.1039/c7fd00117g

Electroactive materials and their applications are enjoying renewed attention, in no small part motivated by the advent of nanoscale tools for their preparation and study. While the fundamentals of charge and mass transport in electrolytes on this scale are by and large well understood, their interplay can have subtle manifestations in the more complex situations typical of, for example, integrated microfluidics-based applications. In particular, the role of faradaic processes is often overlooked or, at best, purposefully suppressed *via* experimental design. In this introductory article we discuss, using simple illustrations from our laboratories, some of the manifestations of electrochemistry in electroactive materials.

1 Introduction

What do electrotunable wetting, electroosmosis, electroactuators, potential-dependent friction and electrovariable plasmonics have in common? All rely on the application of electrical forces to control the properties and/or the dynamics of matter, most commonly fluids or soft materials near the solid–liquid interface. They are also based on the same underlying principles, most notably the physics of electrical screening in electrolytes and the pervasiveness of so-called electrical double-layers (EDLs). Finally, they are research areas currently enjoying a renaissance. This is in no small part due to many of the underlying processes intrinsically taking place at nanometer dimensions. The explosion over the last decades in our ability to create, probe and manipulate matter on this scale has created opportunities for deepened understanding and new applications that are now being avidly explored.

[a]*MESA+ Institute for Nanotechnology, University of Twente, PO Box 217, 7500 AE Enschede, The Netherlands. E-mail: S.G.Lemay@utwente.nl*

[b]*Department of Chemical Engineering, Delft University of Technology, Van der Maasweg 9, 2629 HZ Delft, The Netherlands*

† These authors contributed equally.

The breadth of topics that fall under the umbrella of "chemical physics of electroactive materials" is enormous and would be difficult to address in detail here, and we will not attempt to do so. Instead we will focus on one aspect that extends across many sub-areas, namely, the role played by electron transfer reactions in electroactive systems. Our motivations are twofold. First, we argue that electrochemical processes effectively add an additional dimension to the complex manifold of phenomena occurring in nanoscopic electroactive materials and systems. In particular, whereas the better known effects and applications can usually be understood by treating ions as indestructible particles with a fixed charge, electrochemical processes allow the creation, annihilation or mutual transformation of these charge carriers to at least as great an extent as their solid-state counterpart, electrons and holes in semiconductors. Yet this capability has so far received limited attention in studies of electroactive materials and systems. Second, it has been our experience that electrochemical processes tend to be downplayed or neglected in discussions of electroactive effects. This is often reasonable as many experiments are designed to purposefully marginalize or even eliminate the role of electrochemistry. While this is rational when aiming at minimizing experimental complexity, it can also represent a self-imposed limitation. We hope through the brief exposition below using simple examples for our laboratories to stimulate the reader to reflect on how charge-transfer reactions can influence – or, better yet, create new opportunities – in his or her area(s) of specialization.

2 Electroosmosis & electrochemistry

At the heart of many electroactive materials and processes is the coupling between charge transport by ions and convection of the solvent.[1–5] This includes first and foremost electroosmosis, in which uncompensated charge in a liquid (most notably as occurs in the EDL near a charged surface) allows electric fields to cause solvent transport. It also includes its converse, streaming currents, in which convective transport of a fluid results in electrical currents in the presence of uncompensated charge. Streaming currents can in turn give rise to charge separation on the macroscopic scale and the appearance of streaming potentials. Whether streaming currents or potentials dominate depends on the boundary conditions for ionic charge transport – that is, on the extent to which electrochemical processes are allowed to act as sources or sinks for ionic charge.

While well understood, the principles of electroosmosis are somewhat more subtle than is often implied in the literature; because it serves as an entry to our topic, we take a moment to illustrate this point. Consider perhaps the simplest example, that of electrophoresis of a charged mesoscale entity (*e.g.*, a synthetic microsphere or a macromolecule) suspended in salt water and subject to an externally imposed electric field. The particle drifts at constant velocity, the electric force from the electric field being opposed by a drag force from the fluid. While this simple description is intuitive (and indeed correct), it is still often mistakenly interpreted as stating that the electric force, $F_{\mathrm{el}} = QE$, where Q is the total charge of the particle and E is the magnitude of the electric field, is opposed by Stokes drag, $F_{\mathrm{drag}} = bv$, where b is the Stokes drag coefficient and v is the speed of the particle. This however leads to predicted electrophoretic mobilities $\mu \equiv v/E = Q/b$ which systematically overestimate the experimentally observed

value. This discrepancy is often cast in terms of a reduced "effective charge". While this may provide a way of parameterizing empirical observations, one should not be misled since the discrepancy in fact has its roots in a mistaken assumption about the drag component! To see why, consider the fact that *no net force is applied to the fluid by the electric field*: the force exerted on the charge of the particle is compensated by an equal and opposite electrical force on its EDL. Motion of the particle entails shedding counterions in the wake of the particle and replacing them with new ions from the forward direction, in effect setting up an electroosmotic flow in the reference frame of the particle. Consequently, the particle does not experience simple Stokes drag as it would under the influence of a gravitational or magnetic force, and the viscous forces that it experiences are strongly amplified by the existence of its EDL. This is the basic reason why, for example, DNA molecules of different lengths have comparable electrophoretic mobilities in free solution and that gel separation techniques had to be developed.[6,7] This can be observed directly in experiments by measuring the electrophoretic force on a microscopic object in different electrolytes or in different degrees of confinement.[7–11]

In the above description of electrophoresis we have assumed a constant, uniform external electric field. Since such a field causes ions in the electrolyte to migrate, leading to a net current, this implicitly assumes that charge can be introduced into and extracted from the solution far from the object being studied. This is normally achieved using electrochemical reactions at electrodes immersed in the fluid.[12] Consider for example the widely used Ag/AgCl electrode, which consists of a silver wire coated with a layer of silver chloride. Upon the application of a sufficiently negative potential to the electrode, Cl^- ions are released into solution, leaving behind a neutral Ag atom in the electrode:

$$\mathrm{AgCl\ (solid)} + e^- \rightleftharpoons \mathrm{Ag\ (solid)} + \mathrm{Cl^-\ (aqueous)} \quad (1)$$

The electrons (as well as the energy for powering the electrical current through the solution) are provided by an external power supply. In order to close the electrical circuit, the reverse reaction can take place at a second electrode which then acts as a sink for Cl^- ions. A different electron-transfer reaction can also be employed at the second electrode. In either case this creates a closed circuit for electronic charge, but not for ions. Consequently, ions are either accumulated or depleted in the vicinity of the electrodes (we will return to this important point in Section 3).

Our basic intuition about electrophoresis is further challenged by an electrochemical phenomenon demonstrated just over a decade ago: the autonomous movement of microrods consisting of gold and platinum segments and immersed in aqueous solution containing hydrogen peroxide.[13] This combination of materials and reagents allows different electrochemical reactions to be catalyzed at the surface of the rods, as summarized in Fig. 1a. The reactions in turn cause directed motion along the axis of the rods, as shown in Fig. 1b. This linear motion is superimposed with random rotational diffusion, although later works demonstrated control over the motion by incorporating magnetic materials into the rod structure to allow steering with an external field.[14,15] The propulsion mechanism was originally attributed to an interfacial tension gradient resulting from the formation of oxygen at the platinum end of the rods.[16] In this scenario the

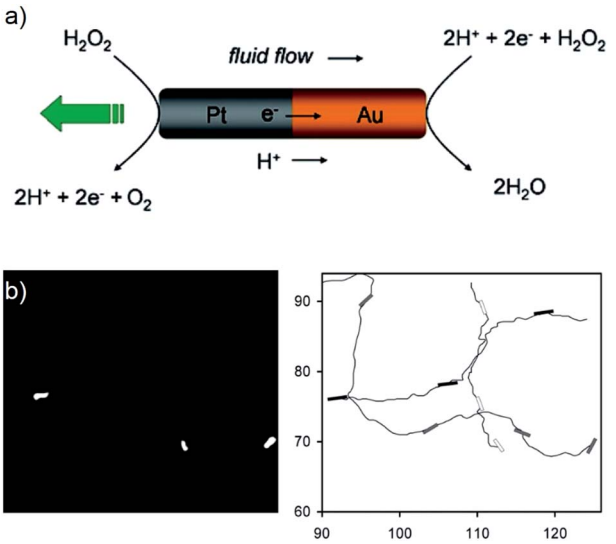

Fig. 1 (a) Schematic illustration of coupled electrochemical reactions leading to self-electrophoresis. At the Pt end of a bimetallic microrod, hydrogen peroxide is oxidized to generate protons in solution and electrons in the wire. The protons and electrons are then consumed *via* the reduction of H_2O_2 at the Au end. The resulting ion flux induces motion of the rod relative to the fluid, propelling it toward the platinum end. Reprinted with permission from W. F. Paxton, P. T. Baker, T. R. Kline, Y. Wang, T. E. Mallouk and A. Sen, *Journal of the American Chemical Society*, 2006, **128**, 14881–14888.[13] Copyright 2006 American Chemical Society. (b) Optical image (left) and plots (right) of the trajectories of 2 μm long platinum/gold microrods in 2.5% aqueous hydrogen peroxide over 5 seconds. While the instantaneous motion is linear, rotational diffusion causes the particle trajectories to meander on the second time scale. Reprinted with permission from W. F. Paxton, K. C. Kistler, C. C. Olmeda, A. Sen, S. K. St. Angelo, Y. Cao, T. E. Mallouk, P. E. Lammert and V. H. Crespi, *Journal of the American Chemical Society*, 2004, **126**, 13424–13431.[24] Copyright 2004 American Chemical Society.

reaction taking place at the gold end merely serves as a means of extracting the electrons generated by the first reaction and preventing charging of the rod (that is, turning it into a bipolar electrode[17]). More elaborate experiments however indicated that the motion in fact results from electrophoretic forces caused by the electrocatalytic reactions.[13,18–20] Protons are generated at the Pt through the decomposition of hydrogen peroxide into water and oxygen and consumed again at the Au. This leads to excess charge and an accompanying electric field that couples to the electrical double layer around the rod and induces motion by self-electrophoresis. While this situation may appear reminiscent of the unphysical feat of "pulling oneself up by one's boot straps", the same basic ingredients are present here as in conventional electrophoresis: the creation of a charge imbalance *via* electrochemical reactions, the consequent development of an electric field along the surface of the rod, and the resulting shearing of the fluid in the EDL of the microrod. The main differences are that charge does not flow *via* an external circuit but instead travels locally along parallel electronic and ionic pathways, and that the energy for this process is provided by molecules present in solution around the particle rather than an external supply. Ensembles of such

self-powered swimmers represent an example of so-called synthetic active matter.[21–23]

While catalytic propulsion was originally observed in the context of the autonomous movement of colloidal microscale objects, it was quickly pointed out that the same mechanism also operates if the bimetal system is anchored to a surface. In this case the bipolar electrode remains motionless and instead the fluid is advected along its surface. This effectively creates a local pump driven by catalytic reactions taking place on the surface.[25–29] In the original demonstration of this effect, Kline *et al.*[30] employed suspended polystyrene (PS) microparticles to visualize the convective flow created above the surface of patterned electrodes. We illustrate the same phenomenon in Fig. 2. Panel (a) shows macroscopic patterns of platinum (forming the letters "NSM") deposited on a gold surface. Upon exposure to an aqueous 3% hydrazine solution, amine-functionalized 1 μm PS colloidal particles close to the gold surface migrate toward the Pt electrode (at a speed of $\sim$3.5 μm s^{-1}), as expected for hydrazine oxidation at the Au surface.[31] Beads reaching the Pt pattern become attached to it, such that within 5 minutes the pattern is covered with beads, as illustrated in Fig. 2b. This concerted movement of beads toward the pattern continues uninterruptedly, eventually leading to multilayer bead formations on top of the platinum feature. Oppositely charged carboxylic-group-modified PS beads were instead found to be repelled from the Pt electrode, in agreement with the observations of Ibele *et al.*[31]

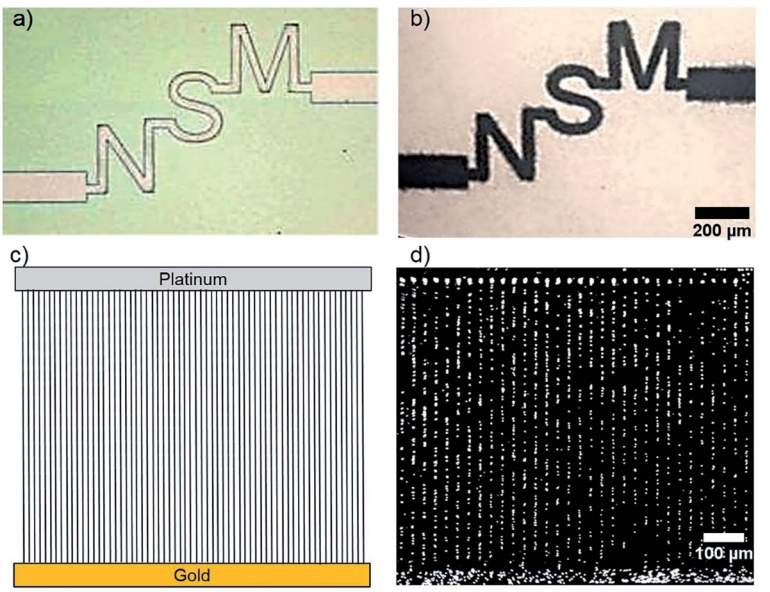

Fig. 2 (a) Microfabricated platinum pattern defined on a gold-covered silicon chip. (b) The platinum pattern becomes covered with multilayers of PS beads after being immersed in an aqueous solution of hydrazine and PS beads. (c) Schematic illustration of alternative pattern for catalytically induced bead manipulation. The array consists of two electrodes (gold and platinum, 30 μm wide) connected *via* passivated 2 μm wide chromium stripes. (d) Laser scanning confocal microscope images of fluorescent PS beads aligned on array when immersed in 3% hydrazine/PS bead aqueous solution.

Interestingly, adding even a low concentration of KCl (10^{-4} M) was sufficient to completely eliminate collective bead motion toward or away from the Pt electrode and restore the unbiased Brownian motion of individual beads. These observations are consistent with an electrophoretic mechanism based on the catalytic consumption of fuel, in this case hydrazine, whose asymmetric decomposition causes an electric field to be generated near the surface. This field superimposes an electrophoretic component to the beads' convective movement and drives them towards or away from the platinum pattern depending on the relative sign and magnitudes of the charges on the surface and on the particles.

Fig. 2c shows another example, a structure consisting of two 30 μm wide electrodes (one Au and one Pt) connected *via* 2 μm wide passivated chromium stripes. When the array is exposed to functionalized PS beads suspended in 3% hydrazine aqueous solution, the beads stream over the surface of the array and become arranged in rows that followed the Cr connecting wires, as illustrated in Fig. 2d.

In Fig. 2, the motion of the fluid was generated on a scale comparable to that of the catalytically active regions. It is however also possible to create a large scale motion *via* the concerted action of multiple local electrochemical actuators. This

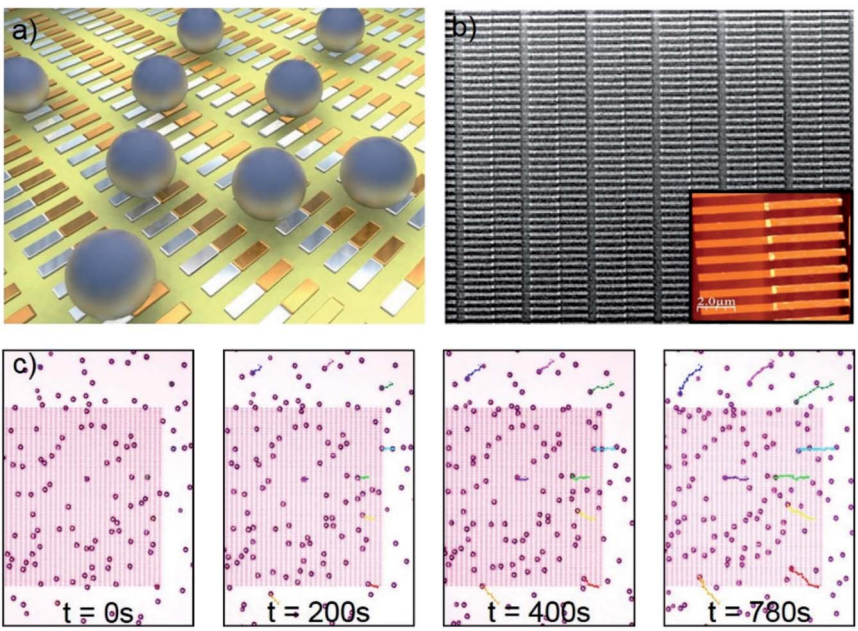

Fig. 3 (a) An artist's impression of the catalytical pump based on a large array of nanoscale propulsion elements. (b) Scanning electron microscope and atomic force microscope (inset) images of platinum/gold microrods that were lithographically defined on an insulating surface (silicon chip with a thermally grown SiO_2 layer). The array contains approximately 58 000 microrods per mm^2 (total catalytically active surface area of approximately 0.23 mm^2), each rod consisting of 4 μm long bands of Au and Pt overlapping by approximately 200 nm to form an electrical contact. (c) Time-lapse images of catalytically induced fluid pumping. The microrod array is visible in the middle of each frame (pink stripes). The trajectories of several of the beads as a function of time are marked on each image using colored lines.

is illustrated in Fig. 3 *via* a massive array of nanofabricated bi-metal (gold/platinum) rods. When the array is exposed to a solution of PS beads (8 μm, zeta potential −46 mV) suspended in 3% H_2O_2 aqueous solution, collective motion of the beads in the surrounding fluid develops. The negatively charged beads are transported with an average speed of 5 μm min^{-1}; the tracking of individual beads, as marked in Fig. 3c, clearly indicates a non-Brownian character for this motion, with most beads exhibiting macroscopically linear trajectories. Over the array this motion is preferentially oriented along the Au/Pt axis, as expected; this motion is superimposed unto an overall radial motion of beads towards the array, reminiscent of macroscopic patterns reported previously.[30–32]

We note that several precautions were found to be necessary to perform reliable bead-tracking experiments. Convection driven by, for example, heating from the imaging microscope or the formation of gas bubbles can easily lead to non-Brownian bead trajectories. The experiments sketched here were performed in 1 mm thick circular adhesive fluid cells (CoverWell, 20 mm diameter) pressed against glass cover slips and containing the substrate under study so as to minimize convection and fluid evaporation.

The examples above represent situations in which electrode materials and reagents were specifically selected for their catalytic activity, leading to pronounced catalytic self-propulsion and pumping effects. In principle, however, the underlying causes for this behavior are generic and can also unintentionally occur in a wide range of micro- and nanofluidics experiments. In addition to purposefully introduced redox-active molecules, local currents and associated flows can be caused by unsuspected reactions involving dissolved oxygen, hydronium ions, and a host of parasitic reactions involving sample impurities. Disconnected electrodes cannot automatically be assumed to be inactive since they can still function in a bipolar fashion, much like the catalytic swimmers described above. Fortunately these effects can be largely eliminated, but doing so conclusively requires good understanding and very careful experimental design.

3 Ionic transport in nanoscale systems

We now leave behind electroosmotic effects to concentrate on processes associated purely with charge transport. The physics of ionic transport bear many similarities to electron and hole transport in semiconductors. Just as the ability to locally dope semiconductors allows creating devices such as diodes and bipolar transistors, manipulation of fixed charges in electrolyte systems leads to rich behavior characterized by spatially inhomogeneous ion distributions and tunable transport properties. We first briefly summarize well-known results on ion concentration polarization, then introduce electrochemical nanofluidics devices and discuss possible analogies involving faradaic processes.

3.1 Ion concentration polarization

The transference number, t_i, is the fraction of the total current density carried in an electrolyte by ionic species i. In a uniform bulk electrolyte, this quantity depends only on the composition of the electrolyte and the mobilities of the different species i. Transference numbers that differ strongly from bulk electrolyte values can occur in permeable materials such as the polyelectrolytes used in

ion-exchange membranes. By virtue of its definition, t_i does not in general lend itself readily to describing systems in which significant concentration gradients occur. In micro- and nanosized channels, however, where equilibration across the cross-section of the channel can take place rapidly, it is convenient to think of the transference number as reflecting the fraction of the total current through the channel carried by species i (that is, the current density associated with the flux of species i integrated over the channel cross-section). In this case t_i represents an effective, one-dimensional transference number that can differ from bulk values and vary with position since charge present on the channel walls leads to an EDL and an excess of counterions.[33] The magnitude of this asymmetry increases with decreasing channel size and the accompanying increase in surface-to-volume ratio; it becomes particularly pronounced when the diffuse components of the EDLs start to overlap (for weakly charged surfaces) or, more generally, when the counterion charge in the compact layer starts to exceed that in the bulk.[34]

Interestingly, interfaces between domains with different transference numbers, independently of how this is physically achieved, tend to exhibit the same basic ion transport behavior. First, their current–voltage characteristics exhibit rectifying behavior. That is, the magnitude of the current is larger for one polarity of the voltage ("forward bias") compared to its opposite ("reverse bias"). Second, and often more significant than the rectifying behavior, the concentration of *both* cations and anions near the interface simultaneously increases (in the forward bias case) or decreases (for reverse bias).

Why this occurs is illustrated in Fig. 4 for the case of a nanochannel containing a junction between positively and negatively charged segments (Fig. 4a). Starting from an equilibrium situation, the application of a positive potential to the right reservoir causes an electrical current to flow from right to left. While the total electrical current is independent of position along the channel, it is carried preferentially by cations moving to the left in the right half of the channel and by anions moving to the right in the left half of the channel. The concentration of both cations and anions near the junction tends to increase as a result of this current. This buildup of ions continues until diffusive gradients compensate for the differences in ion concentration, as shown in Fig. 4b (left panel). If an electric field is applied in the opposite direction, the converse occurs and the junction between the segments becomes depleted of salt (Fig. 4b, right panel). This is directly reflected in the current–voltage characteristics of the junction: while the current tends to increase superlinearly with increasing forward bias due to a decrease in resistivity caused by carrier accumulation, it is highly suppressed in the reverse-biased direction due to depletion (Fig. 4c). This behavior is closely related to that of solid-state p–n junctions, but significant differences exist at the quantitative level. In particular, giant enrichment of both carrier types as shown in Fig. 4b is not as readily realized in semiconductors due to electron–hole recombination, and migration (*i.e.*, ohmic drops, and thus also transference numbers) usually play a more prominent role relative to interfacial potentials in the fluidic case.

The device in Fig. 4 has been coined an ionic or nanofluidic diode,[35–37] a term which has also been applied[38] to conical nanopores,[39–43] asymmetric nanochannels[44] and straight nanochannels connected to reservoirs with asymmetries in solution composition.[45,46] But electroactive systems where domains with different transference numbers are in contact arise much more frequently.

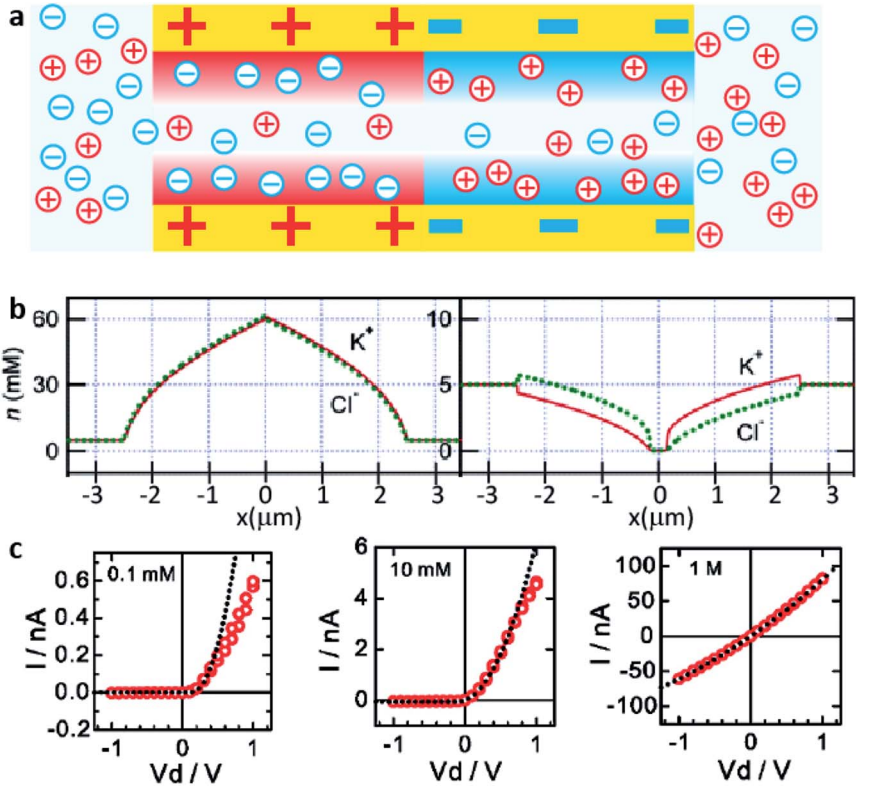

Fig. 4 (a) Sketch of a bipolar nanochannel with positively and negatively charged regions. (b) Calculated concentration profiles for K^+ cations and Cl^- anions under forward (left) and reverse (right) bias of 5 V in a nanochannel of 30 nm height with surface charge densities of 2 mC m^{-2} (left half) and −2 mC m^{-2} (right half). Reprinted with permission from H. Daiguji, Y. Oka and K. Shirono, *Nano Lett.*, 2005, **5**, 2274–2280.[35] Copyright 2005 American Chemical Society. (c) Measured current–voltage characteristics of a nanofluidic diode based on a 20 nm height bipolar channel with surface charge densities of +1.3 and −4 mC m^{-2} at bulk KCl concentrations of 0.1 mM (left), 10 mM (middle) and 1 M (right). Reprinted with permission from L.-J. Cheng and L. J. Guo, *ACS Nano*, 2009, **3**, 575–584.[36] Copyright 2009 American Chemical Society.

Perhaps the simplest example is the interface between a nanochannel and a larger channel or reservoir,[2,47] which provides a broadly applicable route for concentrating analyte molecules based on their charge.[48–53] Conversely, the depletion effect at the micro/nanochannel interface has been exploited in, for example, depletion zone isotachophoresis.[54] More broadly, assemblies of ion-selective porous materials such as microparticle assemblies[55,56] and polyelectrolyte gels[57–59] exhibit similar behavior. These have been exploited for electrical actuation of responsive gels[60,61] and in ion-exchange membranes.[62]

More complex networks involving multiple parallel pathways with different transference numbers can exhibit more complex behavior than simple rectification, including multistability.[63]

3.2 Electrochemical nanofluidics devices

We have seen in Section 3.1 that static spatial inhomogeneities in the cation/anion transport ratio of a medium, as represented by spatially varying transference numbers, can have dramatic and counterintuitive consequences for charge transport, and that these effects are enhanced for high surface-to-volume ratios such as those that occur in nanochannels. The introduction of embedded electrodes to perform electrochemical reactions in nanoscale channels further complicates this picture in two main ways. First, the surface charge at an electrode and the associated influence on transference numbers are no longer static and can instead be tuned *via* an external potential. Other properties such as reversible adsorption of ionic species can also depend on potential.[64,65] Second, ionic species are no longer conserved since redox reactions allow the local creation, annihilation and/or transmutation of ionic species to take place. What are the consequences of these new ingredients is a question that has hardly been broached so far.

For concreteness we focus here on one particular class of electrochemical nanofluidic systems, namely, devices that enable efficient redox cycling between two closely spaced electrodes. Successive reduction and oxidation of molecules present in such devices allows shuttling of electrons between the electrodes at a high rate, leading to orders-of-magnitude signal enhancement compared to conventional voltammetry or amperometry. Such geometries featuring nanoscale distances between the electrodes have been realized using a number of strategies that include, for example, interdigitated electrodes[66–70] and ring-disk electrodes.[71,72] Our group's approach,[65,73–75] which relies on lithography-based

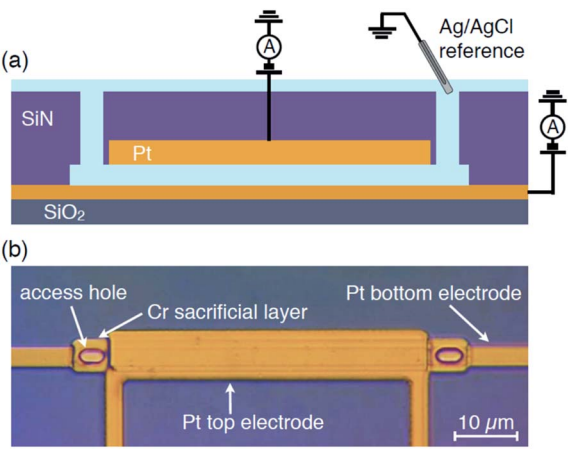

Fig. 5 (a) Schematic cross section of a nanogap electrochemical detector. Redox-active molecules shuttle diffusively between the closely spaced (<100 nm) Pt electrodes, where they are repeatedly oxidized and reduced and generate a highly amplified electrochemical current. (b) Optical micrograph (top view) of a lithographically fabricated device consisting of a 50 μm long and 5 μm wide detection region. The two access holes can be connected to external microfluidic channels to allow pressure-driven flow through the device.[77] Reprinted from *Electrochimica Acta* **112**, K. Mathwig and S. G. Lemay, Mass transport in electrochemical nanogap sensors, 943–949, Copyright (2013), with permission from Elsevier.[78]

microfabrication techniques, is illustrated in Fig. 5. The core device consists of a nanochannel (height ~40–70 nm, width ~2–5 μm, length ~10–100 μm) whose floor and ceiling consist of separately addressable electrodes. Details of the device fabrication process have been described elsewhere.[65,76] In such a geometry, the diffusion-limited redox cycling current between the two electrodes (*i.e.*, the expected current assuming high overpotentials for both reduction and oxidation) is

$$I_{\mathrm{rc}} = \frac{neA}{z}\left(\frac{2D^{\mathrm{RED}}D^{\mathrm{OX}}}{D^{\mathrm{RED}}+D^{\mathrm{OX}}}\right)\overline{C}. \quad (2)$$

Here, n is the number of electrons shuttled per cycle, e is the electronic charge, A is the area of overlap of the two facing electrodes, z is the separation between the electrodes, $\bar{C}$ is the average concentration of redox molecules in the volume between the electrodes, and D^{RED} and D^{OX} are the diffusion coefficients of the reduced and oxidized species, respectively. This expression motivates the interest in nanodevices as the detected signal is inversely proportional to the electrode spacing z.

Bringing a target analyte into such a device can rely either on passive diffusion from an external "bulk" reservoir or on an actively controlled advective flow along the channel.[77] In the latter case, an important property resulting from the high aspect ratio between the height of the channel and the length of the electrodes is that the redox cycling gradient between the electrodes is established on much faster time scales than advection through the device. Consequently, the redox cycling gradient is not significantly disturbed by convection, except at extreme (and so far unachievable) flow rates.[78] More precisely, the Graetz number, Gz, is a dimensionless quantity that characterizes the ratio of the diffusion time across the cross-section of the channel to the advection time along the length of the electrode. For our rectangular cross-section its value is given by $\mathrm{Gz} = z^2v/DL$, where v is the average flow speed and L is the length of the detection region. For typical parameters $z = 50$ nm, $v = 100$ μm s^{-1}, $D = 0.5 \times 10^{-9}$ m^2 s^{-1} and $L = 100$ μm, this yields $\mathrm{Gz} = 5 \times 10^{-6} \ll 1$ and the diffusion profile between the electrodes is fully established.

Early experiments using such nanoscale devices focused on exploiting the high charge amplification resulting from redox cycling to probe the underlying microscopic charge transport dynamics. Relatively small numbers of molecules are present in the detection region between the two electrodes at any given time because of the small volume involved (order of a few femtoliters). Since the redox cycling current is directly proportional to the number of such molecules, equilibrium statistical fluctuations around the mean number of molecules can be detected as current noise. An important signature of such noise, illustrated in Fig. 6a, is that the current fluctuations are essentially identical at the reducing and oxidizing electrodes since both currents are caused by the same molecules shuttling between the electrodes. The rate at which such fluctuations take place, as characterized by the noise spectral density[74,79] or its time-domain equivalent, the autocorrelation function,[77] reflects the speed with which molecules enter and leave the detection volume. This approach can be extended down to pM concentrations, at which point the noise consists of telegraph-like signals corresponding to individual molecules entering and exiting the detection region (Fig. 6b).

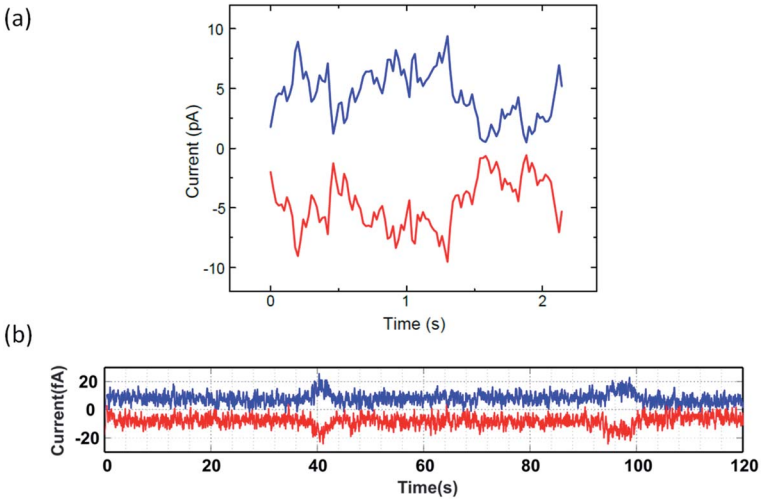

Fig. 6 (a) Fluctuations in the redox cycling current obtained for 100 μM $Fc(MeOH)_2$ in an aqueous electrolyte due to equilibrium statistical fluctuations of the number of molecules present in the detection volume. The DC component has been offset to focus on the fluctuations. The currents for the oxidizing (blue) and reducing (red) electrodes are strongly correlated but have opposite signs, as expected for redox cycling. Reprinted with permission from P. S. Singh *et al.*, *J. Am. Chem. Soc*, 2011, **133**, 18289–18295. Copyright 2011 American Chemical Society.[64] (b) Corresponding current–time traces for 10 pM $FcTMA^+$. At such low concentrations, less than one redox molecule is present on average in the detection volume. The entry and departure of individual molecules appear as plateaus in the ultra-low (fA-level) current signals. Here two particularly long events can be observed near 40 s and 95 s. Reprinted with permission from S. Kang *et al.*, *ACS Nano* 2013, **7**, 10931–10937. Copyright 2013 American Chemical Society.[75]

A surprising – and still somewhat controversial – finding from these measurements was that outer-sphere redox couples such as ferrocene derivatives appear to exhibit a significant degree of reversible adsorption to metal electrodes.[64,79,80] These observations are also consistent with studies of the temporal response of nanogap sensors[65] and the smaller-than-expected current signature of single molecules during redox cycling.[74,75] Although such molecule-surface interactions are too weak to be readily detected in conventional micro- or macroscale systems, they become very significant in <100 nm high channels due to the high surface-to-volume ratio.

The analysis performed to date to interpret microscopic data such as those sketched here has focused on simple models based on diffusion and advection. As we discuss in the next section, however, this neglects indirect forms of interactions that may play a role in more complex multi-electrode fluidic systems.

3.3 Electrochemically induced concentration polarization

To illustrate the parallel between electrochemical reactions and the enrichment/depletion effects discussed in Section 3.1, we first consider the trivial case of two conventional Ag/AgCl electrodes (as described by eqn (1)) immersed in two large reservoirs that are connected *via* a small channel and filled with KCl. Within the electrolyte, the contributions to the total electrical current carried by K^+ cations

and Cl^- anions are comparable ($t_K \approx t_{Cl} \approx 0.5$). At the electrolyte/electrode interface, on the other hand, only Cl^- ions are exchanged and the transference numbers characterizing this interface are thus $t_K \approx 0$, $t_{Cl} \approx 1$. In analogy with the mechanism of Fig. 4, driving a DC current through the channel results in the net accumulation of both cations and anions at one liquid–electrode interface and their depletion at the other. This is usually negligible on the scale of most nanofluidics experiments, in which the currents, being limited by the resistance of the nanochannel, are small and the concentrations in the reservoirs are sufficiently large that they are not significantly perturbed on experimental scales. For example, a 1 nA current, which represents a significant faradaic current at a microscale electrode, takes $\sim 10^7$ s to perturb the concentration of a 100 μL, 0.1 M KCl reservoir by only 1%.

What if the reservoirs are miniaturized or if redox reactions take place in a small isolated volume? Consider a simple thought experiment, illustrated in Fig. 7, in which a long, thin, sealed channel contains a simple electroactive species that can exist in two charge states, reduced (RED) and oxidized (OX). As sketched in Fig. 7a, electrodes of length L_e are situated in the walls of this channel so as to define two domains separated by a gap of length L_g in which no electrode is present. Switching the potential of the electrodes between two voltages, V^{RED} and V^{OX}, insures that the molecules near each electrode quickly reach electrochemical equilibrium and attain a well-defined state: RED or OX. Any change in the total charge within the system as a result of switching the potential of the electrodes is assumed to be compensated by inert supporting salt ions diffusing into the channel, also screening out electric fields beyond the electrodes' EDLs. In the initial phase of the experiment, both the left and the right domain are biased at potential V^{RED}. All molecules are in the RED state, and the concentration of molecules is uniform throughout the system. At the particular moment $t = 0$, the potential of the left electrode is switched to potential V^{OX}, switching the redox molecules in this domain to the OX state. Counterbalancing concentration gradients of molecules in RED and OX states are set up between the two electrode domains. So long as the molecules are indistinguishable apart from their redox state, the resulting concentration profiles are symmetric, as sketched in Fig. 7b. In practice, however, the diffusion coefficients D^{RED} and D^{OX} for the two redox states are usually not identical. In this case the situation in Fig. 7b is not in steady state, as the flux of molecules in the OX state diffusing from left to right ($D^{OX}(dC^{OX}/dx)$) is less than that of particles in the RED state diffusing from right to left ($D^{RED}(dC^{RED}/dx)$). A net migration of particles from left to right then takes place until a new equilibrium is achieved in which the concentration in the left reservoir is lower than that in the right reservoir, as sketched in Fig. 7c. This illustrates how electrochemical reactions provide a pathway for the establishment of concentration imbalances. Importantly, the relative imbalance in the equilibrium concentrations, $C^{OX}/C^{RED} = D^{RED}/D^{OX}$, is independent of the device dimensions. The characteristic relaxation time toward equilibrium, which is diffusion limited and thus given roughly by $[\max(L_g,L_d)]^2/[D^{OX} + D^{RED}]$, on the other hand, is geometry dependent. For $L_e = L_g = 10$ μm and typical diffusion coefficients of order 0.5×10^{-9} m^2 s^{-1}, the relaxation time yields an order of 0.1 s, a time scale which is short enough to interfere with many measurements.

The thought experiment of Fig. 7 calls for a completely isolated volume and is therefore difficult to implement in practice. For open systems, as typical in most

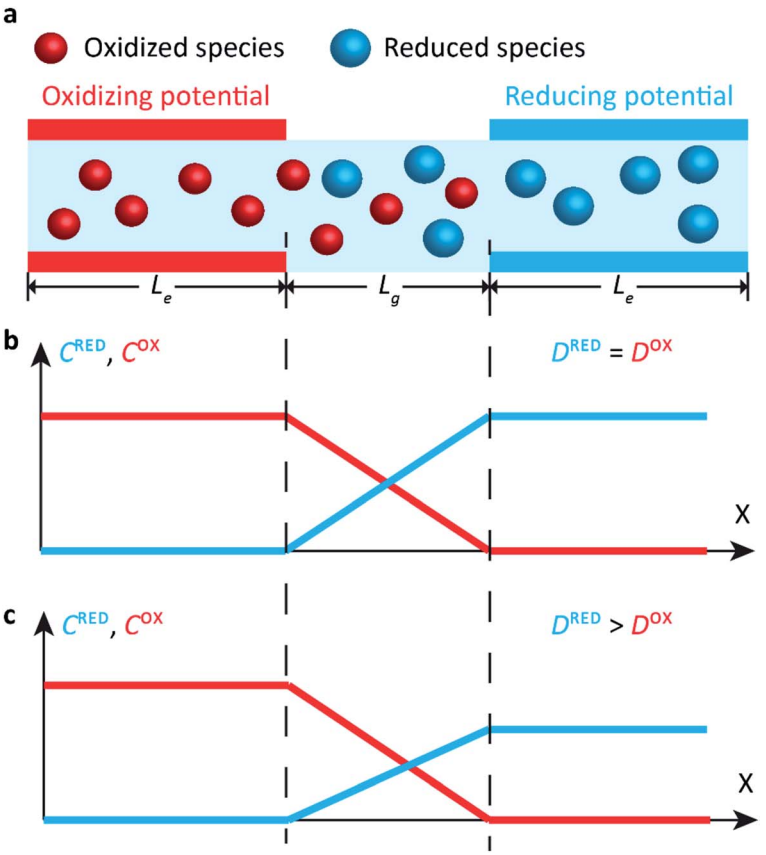

Fig. 7 Thought experiment illustrating electrochemically induced concentration polarization. (a) Sketch of a sealed nanochannel in which the redox state of molecules can be switched between a reduced (RED) and an oxidized (OX) state using electrodes (red and blue bands). Here we take the left electrode as oxidizing and the right electrode as reducing. (b) Concentration of RED and OX molecules *versus* longitudinal position along the channel when the diffusion coefficients D^{RED} and D^{OX} are equal. The total concentration of redox molecules is uniform throughout the channel. (c) Same as (b) but with $D^{RED} > D^{OX}$. An asymmetry develops in the concentration profiles with a higher total concentration being present at the oxidizing electrode.

fluidic experiments of the sort sketched in Section 3.2, the interpretation is instead more tricky because equilibration with the external reservoirs must be taken into account.[81] This can however be circumvented *via* the application of a flow along the channel. To illustrate this point, we show the results of an experiment involving a device analogous to that discussed in Section 3.2 which is sketched in Fig. 8a. It consists of a channel (height 90 nm, width 5 μm) supporting a pressure-driven flow (average advection velocity, v). Two electrode pairs embedded in the floor and ceiling of the channel (dimensions as indicated in Fig. 8a) allow controlling the redox state of the molecules in the vicinity of the electrodes. Setting one of the top electrodes to an oxidizing potential and the corresponding bottom electrode to a reducing potential allows redox cycling

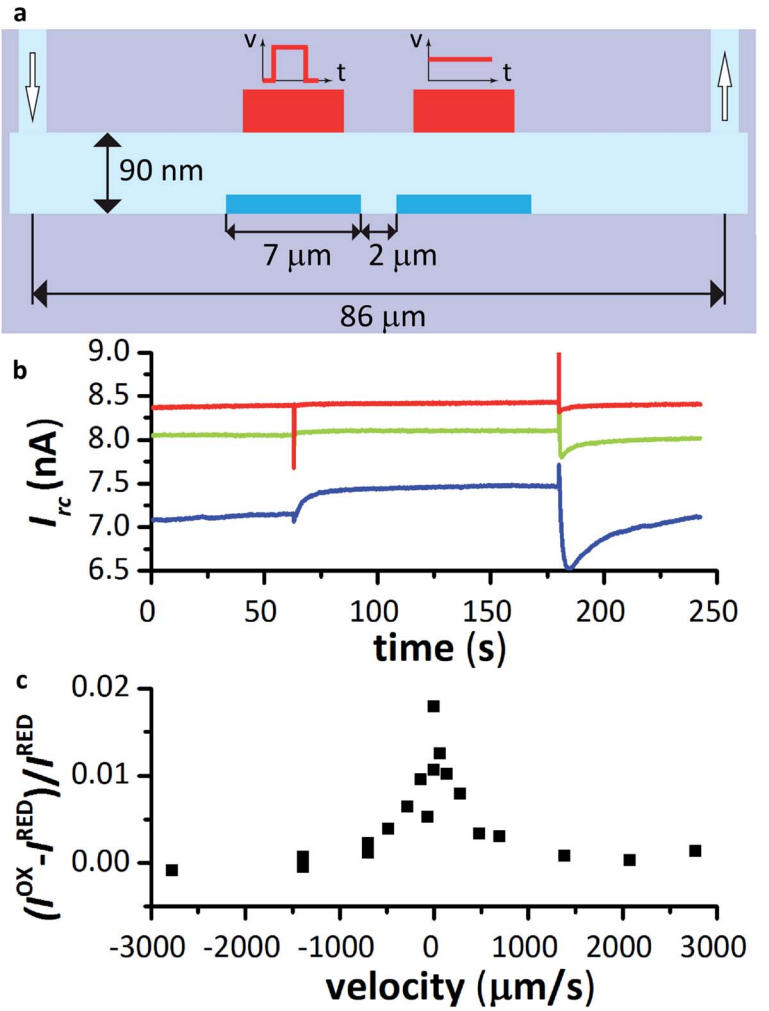

Fig. 8 (a) Electrochemical nanofluidics device consisting of two pairs of electrodes spanning a nanofluidics channel, as described in the main text. The potential of the top left electrode is switched between reducing and oxidizing potentials while the average concentration of redox-active molecules is monitored at the right pair of electrodes *via* the redox cycling current, I_{rc}. (b) Current–time response at the right electrode pair for three fluid velocities (0, 270 and 2000 μm s^{-1} for the blue, green and red curves, respectively). The potential of the top left electrode is switched near 60 s and 180 s, causing the steady-state concentration to change at the position of the right electrode pair. (c) Relative shift in steady-state concentration at the right electrodes as a function of fluid velocity. The coupling between the electrodes vanishes at both positive and negative high velocities.

between the facing electrode pairs and the redox cycling current, I_{rc}, is then determined using eqn (2).

Switching the potential of one electrode between reducing and oxidizing potentials causes the relative concentration of molecules in the RED and OX states to change locally, creating a scenario analogous to that of Fig. 7 (with the

minor difference that the concentration in the redox cycling regions is a mixture of RED and OX instead of pure RED or OX). A change in the spatial distribution of redox molecules caused by this potential switch can be detected *via* redox cycling at a second electrode pair elsewhere in the channel. This is illustrated experimentally in Fig. 8b, where the redox-cycling current at the right pair of electrodes is shown as a function of time while the top left electrode has its potential switched between a reducing and an oxidizing potential (both bottom electrodes remain at reducing potentials throughout). Following each switch in potential of the top left electrode (marked by a sudden spike), the current at the right electrode pair undergoes a slow transient before settling to a new value. Both the duration of the transient and the difference in steady-state current levels depends on the flow rate of the solution, with high flow rates leading to more ideal behavior. This is summarized in Fig. 8c, which shows the relative magnitude of the change at the remote electrode pair as a function of the average flow velocity. The potential of a left-side electrode influences the average concentration $\bar{C}$ at the right electrode pair, independently of which electrode is upstream of the other (the large scatter close to $v = 0$ is due to the fact that we cannot establish a true steady state in the nanofluidics channel at such low velocities).

What sets the velocity scale over which the "non-local" influence of an electrode on its neighbor vanishes? Steady-state solutions of the drift-diffusion equation, $\partial c/\partial t = D\partial^2 c/\partial x^2 - v\partial c/\partial x$, have the general form $c(x) = A + B\exp(vx/D)$, indicating that electrodes stop influencing each other when sufficiently far apart or at sufficiently high velocities. For a gap between the electrodes of length $L_g = 2$ μm and a typical diffusion coefficient $D \approx 0.5 \times 10^{-9}$ m^2 s^{-1}, the crossover is expected at an advection velocity of $v = D/L_g \approx 250$ μm s^{-1}, in qualitative agreement with the experimental observations (equivalently, the Peclet number $\mathrm{Pe} = L_g v/D$ is unity at $v \approx 250$ μm s^{-1}). This suggests that the observed changes in redox cycling signal away from the electrode at which electrochemical actuation takes place are indeed due to a re-organization of the concentration profile in the device.

4 Outlook

The majority of studies of electroactive materials and systems concentrate on scenarios in which ions play the role of indestructible mobile charge carriers. The existence of cations and anions as separate, parallel pathways for charge transport, the inherent coupling between ionic charge transport and solvent motion, and the ability to control either surface charge (for channel-based systems) or bulk charge density (for permeable materials) leads to a rich range of physical effects that spans classic electroosmosis, ion-selective membranes, tunable tribological and optical properties, nonlinear transport at interfaces, actuation, and more.

In this context, electrochemical reactions often represent unwanted parasitic pathways for charge that one attempts to eliminate or circumvent through a judicious choice of materials, solution composition, or applied potentials. Conceptually, however, electrochemical reactions represent an extension of the range of available boundary conditions for charge transport. Do qualitatively new effects exist as a result of these additional forms of coupling? Do these provide a significant advantage for applications? What seems certain at this moment is

that, insofar as such effects exist, they can be expected to become increasingly relevant upon downscaling the dimensions of a system and thus increasing its surface-to-volume ratio.

On a more mundane level, the practical experience of many researchers performing electrical transport experiments in micro- and nanofluidics includes dealing with slow drift in measured signals. Colloquial evidence suggests that the use of even low-frequency AC signals alleviates many of the symptoms. This behavior is often attributed to unspecified chemical changes, for example, at the surfaces being studied. While this is no doubt a significant factor in many experiments, such behavior is also a hallmark of concentration polarization effects, whether externally driven (Section 3.1) or the result of changes in redox states (Section 3.3). Even leakage currents through poor insulation can in principle lead to significant concentration changes over a long period of time if no mechanism exists to equilibrate concentrations, as is often the case in confined fluidic systems.

We conclude that achieving further awareness of possible faradaic effects in electroactive systems is a worthwhile pursuit. This is true whether one's main motivation is seeking insurance against the proverbial "wolf under the bed" in an experiment, or seeking to expand the battery of experimental knobs available. Both are worthwhile causes, and we urge the reader to remember faradaic processes when contemplating either.

References

1 T. M. Squires and S. R. Quake, *Rev. Mod. Phys.*, 2005, **77**, 977–1026.
2 R. B. Schoch, J. Y. Han and P. Renaud, *Rev. Mod. Phys.*, 2008, **80**, 839–883.
3 W. Sparreboom, A. van den Berg and J. C. T. Eijkel, *Nat. Nanotechnol.*, 2009, **4**, 713–720.
4 L. Bocquet and E. Charlaix, *Chem. Soc. Rev.*, 2010, **39**, 1073–1095.
5 S. Wall, *Curr. Opin. Colloid Interface Sci.*, 2010, **15**, 119–124.
6 J. L. Viovy, *Rev. Mod. Phys.*, 2000, **72**, 813–872.
7 T. N. Shendruk, O. A. Hickey, G. W. Slater and J. L. Harden, *Curr. Opin. Colloid Interface Sci.*, 2012, **17**, 74–82.
8 S. van Dorp, U. F. Keyser, N. H. Dekker, C. Dekker and S. G. Lemay, *Nat. Phys.*, 2009, **5**, 347–351.
9 A. R. Hall, S. van Dorp, S. G. Lemay and C. Dekker, *Nano Lett.*, 2009, **9**, 4441–4445.
10 S. Ghosal, *Phys. Rev. E: Stat., Nonlinear, Soft Matter Phys.*, 2006, **74**, 5.
11 D. Long, J. L. Viovy and A. Ajdari, *Biopolymers*, 1996, **39**, 755–759.
12 M. W. Shinwari, D. Zhitomirsky, I. A. Deen, P. R. Selvaganapathy, M. J. Deen and D. Landheer, *Sensors*, 2010, **10**, 1679.
13 W. F. Paxton, P. T. Baker, T. R. Kline, Y. Wang, T. E. Mallouk and A. Sen, *J. Am. Chem. Soc.*, 2006, **128**, 14881–14888.
14 J. Burdick, R. Laocharoensuk, P. M. Wheat, J. D. Posner and J. Wang, *J. Am. Chem. Soc.*, 2008, **130**, 8164–8165.
15 S. Sundararajan, P. E. Lammert, A. W. Zudans, V. H. Crespi and A. Sen, *Nano Lett.*, 2008, **8**, 1271–1276.
16 T. R. Kline, W. F. Paxton, T. E. Mallouk and A. Sen, *Angew. Chem., Int. Ed.*, 2005, **44**, 744–746.

17 S. E. Fosdick, K. N. Knust, K. Scida and R. M. Crooks, *Angew. Chem., Int. Ed.*, 2013, **52**, 10438–10456.
18 M. Pumera, *Nanoscale*, 2010, **2**, 1643–1649.
19 J. L. Moran, P. M. Wheat and J. D. Posner, *Phys. Rev. E: Stat., Nonlinear, Soft Matter Phys.*, 2010, **81**, 4.
20 R. Laocharoensuk, J. Burdick and J. Wang, *ACS Nano*, 2008, **2**, 1069–1075.
21 W. Wang, W. T. Duan, S. Ahmed, A. Sen and T. E. Mallouk, *Acc. Chem. Res.*, 2015, **48**, 1938–1946.
22 M. C. Marchetti, J. F. Joanny, S. Ramaswamy, T. B. Liverpool, J. Prost, M. Rao and R. A. Simha, *Rev. Mod. Phys.*, 2013, **85**, 47.
23 Y. Hong, N. M. K. Blackman, N. D. Kopp, A. Sen and D. Velegol, *Phys. Rev. Lett.*, 2007, **99**, 4.
24 W. F. Paxton, K. C. Kistler, C. C. Olmeda, A. Sen, S. K. St. Angelo, Y. Cao, T. E. Mallouk, P. E. Lammert and V. H. Crespi, *J. Am. Chem. Soc.*, 2004, **126**, 13424–13431.
25 T. R. Kline and A. Sen, *Langmuir*, 2006, **22**, 7124–7127.
26 V. Yadav, H. Zhang, R. Pavlick and A. Sen, *J. Am. Chem. Soc.*, 2012, **134**, 15688–15691.
27 D. Kagan, S. Balasubramanian and J. Wang, *Angew. Chem., Int. Ed.*, 2011, **50**, 503–506.
28 S. Subramanian and J. M. Catchmark, *J. Phys. Chem. C*, 2007, **111**, 11959–11964.
29 J. Zhang and J. M. Catchmark, *Microfluid. Nanofluid.*, 2011, **10**, 1147–1151.
30 T. R. Kline, J. Iwata, P. E. Lammert, T. E. Mallouk, A. Sen and D. Velegol, *J. Phys. Chem. B*, 2006, **110**, 24513–24521.
31 M. E. Ibele, Y. Wang, T. R. Kline, T. E. Mallouk and A. Sen, *J. Am. Chem. Soc.*, 2007, **129**, 7762–7763.
32 T. R. Kline, W. F. Paxton, Y. Wang, D. Velegol, T. E. Mallouk and A. Sen, *J. Am. Chem. Soc.*, 2005, **127**, 17150–17151.
33 A. Plecis, R. B. Schoch and P. Renaud, *Nano Lett.*, 2005, **5**, 1147–1155.
34 D. Stein, M. Kruithof and C. Dekker, *Phys. Rev. Lett.*, 2004, **93**, 4.
35 H. Daiguji, Y. Oka and K. Shirono, *Nano Lett.*, 2005, **5**, 2274–2280.
36 L.-J. Cheng and L. J. Guo, *ACS Nano*, 2009, **3**, 575–584.
37 R. Karnik, C. Duan, K. Castelino, H. Daiguji and A. Majumdar, *Nano Lett.*, 2007, **7**, 547–551.
38 L.-J. Cheng and L. J. Guo, *Chem. Soc. Rev.*, 2010, **39**, 923–938.
39 J. Cervera, B. Schiedt and P. Ramírez, *EPL*, 2005, **71**, 35.
40 I. Vlassiouk, T. R. Kozel and Z. S. Siwy, *J. Am. Chem. Soc.*, 2009, **131**, 8211–8220.
41 Z. Siwy, E. Heins, C. C. Harrell, P. Kohli and C. R. Martin, *J. Am. Chem. Soc.*, 2004, **126**, 10850–10851.
42 L. Wang, W. Guo, Y. B. Xie, X. W. Wang, J. M. Xue and Y. G. Wang, *Radiat. Meas.*, 2009, **44**, 1119–1122.
43 L. Cao, W. Guo, Y. Wang and L. Jiang, *Langmuir*, 2012, **28**, 2194–2199.
44 M. Ali, B. Schiedt, R. Neumann and W. Ensinger, *Macromol. Biosci.*, 2010, **10**, 28–32.
45 L.-J. Cheng and L. J. Guo, *Nano Lett.*, 2007, **7**, 3165–3171.
46 W. Guo, L. Cao, J. Xia, F.-Q. Nie, W. Ma, J. Xue, Y. Song, D. Zhu, Y. Wang and L. Jiang, *Adv. Funct. Mater.*, 2010, **20**, 1339–1344.
47 H. Daiguji, P. Yang and A. Majumdar, *Nano Lett.*, 2004, **4**, 137–142.

48 S. J. Kim, Y. A. Song and J. Han, *Chem. Soc. Rev.*, 2010, **39**, 912–922.
49 T. A. Zangle, A. Mani and J. G. Santiago, *Chem. Soc. Rev.*, 2010, **39**, 1014–1035.
50 K. D. Huang and R. J. Yang, *Electrophoresis*, 2008, **29**, 4862–4870.
51 Y. C. Wang, A. L. Stevens and J. Y. Han, *Anal. Chem.*, 2005, **77**, 4293–4299.
52 Q. S. Pu, J. S. Yun, H. Temkin and S. R. Liu, *Nano Lett.*, 2004, **4**, 1099–1103.
53 S. J. Kim, S. H. Ko, K. H. Kang and J. Han, *Nat. Nanotechnol.*, 2010, **5**, 297–301.
54 J. Quist, P. Vulto, H. van der Linden and T. Hankemeier, *Anal. Chem.*, 2012, **84**, 9065–9071.
55 Y. Lei, W. Wang, W. Wu and Z. Li, *Appl. Phys. Lett.*, 2010, **96**, 263102.
56 E. Choi, C. Wang, G. T. Chang and J. Park, *Nano Lett.*, 2016, **16**, 2189–2197.
57 O. J. Cayre, S. T. Chang and O. D. Velev, *J. Am. Chem. Soc.*, 2007, **129**, 10801–10806.
58 H.-J. Koo, S. T. Chang and O. D. Velev, *Small*, 2010, **6**, 1393–1397.
59 J.-H. So, H.-J. Koo, M. D. Dickey and O. D. Velev, *Adv. Funct. Mater.*, 2012, **22**, 625–631.
60 M. Doi, M. Matsumoto and Y. Hirose, *Macromolecules*, 1992, **25**, 5504–5511.
61 P. J. Glazer, M. van Erp, A. Embrechts, S. G. Lemay and E. Mendes, *Soft Matter*, 2012, **8**, 4421–4426.
62 H. Strathmann, *Ion-Exchange Membrane Separation Processes*, Elsevier, 2004.
63 C. J. C. Biscombe, M. R. Davidson and D. J. E. Harvie, *Microfluid. Nanofluid.*, 2012, **13**, 481–490.
64 P. S. Singh, H. S. M. Chan, S. Kang and S. G. Lemay, *J. Am. Chem. Soc.*, 2011, **133**, 18289–18295.
65 S. Kang, K. Mathwig and S. G. Lemay, *Lab Chip*, 2012, **12**, 1262–1267.
66 D. G. Sanderson and L. B. Anderson, *Anal. Chem.*, 1985, **57**, 2388–2393.
67 O. Niwa, Y. Xu, H. B. Halsall and W. R. Heineman, *Anal. Chem.*, 1993, **65**, 1559–1563.
68 V. A. T. Dam, W. Olthuis and A. van den Berg, *Analyst*, 2007, **132**, 365–370.
69 E. D. Goluch, B. Wolfrum, P. S. Singh, M. A. G. Zevenbergen and S. G. Lemay, *Anal. Bioanal. Chem.*, 2009, **394**, 447–456.
70 J. I. Heo, D. S. Shim, G. T. Teixidor, S. Oh, M. J. Madou and H. Shin, *J. Electrochem. Soc.*, 2011, **158**, J76–J80.
71 C. Ma, N. M. Contento, L. R. Gibson II and P. W. Bohn, *ACS Nano*, 2013, **7**, 5483–5490.
72 G. Zhao, D. M. Giolando and J. R. Kirchhoff, *Anal. Chem.*, 1995, **67**, 1491–1495.
73 M. A. G. Zevenbergen, D. Krapf, M. R. Zuiddam and S. G. Lemay, *Nano Lett.*, 2007, **7**, 384–388.
74 M. A. G. Zevenbergen, P. S. Singh, E. D. Goluch, B. L. Wolfrum and S. G. Lemay, *Nano Lett.*, 2011, **11**, 2881–2886.
75 S. Kang, A. F. Nieuwenhuis, K. Mathwig, D. Mampallil and S. G. Lemay, *ACS Nano*, 2013, **7**, 10931–10937.
76 M. A. G. Zevenbergen, B. L. Wolfrum, E. D. Goluch, P. S. Singh and S. G. Lemay, *J. Am. Chem. Soc.*, 2009, **131**, 11471–11477.
77 K. Mathwig, D. Mampallil, S. Kang and S. G. Lemay, *Phys. Rev. Lett.*, 2012, **109**, 118302.
78 K. Mathwig and S. G. Lemay, *Electrochim. Acta*, 2013, **112**, 943–949.
79 M. A. G. Zevenbergen, P. S. Singh, E. D. Goluch, B. L. Wolfrum and S. G. Lemay, *Anal. Chem.*, 2009, **81**, 8203–8212.

80 D. Mampallil, K. Mathwig, S. Kang and S. G. Lemay, *J. Phys. Chem. Lett.*, 2014, **5**, 636–640.
81 D. Mampallil, K. Mathwig, S. Kang and S. G. Lemay, *Anal. Chem.*, 2013, **85**, 6053–6058.

